

Molecular Determinants of Potent P2X2 Antagonism Identified by Functional Analysis, Mutagenesis, and Homology Docking^[S]

Christian Wolf, Christiane Rosefort, Ghada Fallah, Matthias U. Kassack, Alexandra Hamacher, Mandy Bodnar, Haihong Wang, Peter Illes, Achim Kless, Gregor Bahrenberg, Günther Schmalzing, and Ralf Hausmann

Molecular Pharmacology, RWTH Aachen University, Aachen, Germany (C.W., C.R., G.F., G.S., R.H.); Institute of Pharmaceutical & Medicinal Chemistry, Heinrich-Heine-University Düsseldorf, Düsseldorf, Germany (M.U.K., A.H.); Rudolf-Boehm Institute for Pharmacology and Toxicology, University of Leipzig, Leipzig, Germany (M.B., H.W., P.I.); and Grünenthal GmbH, Global Drug Discovery, Departments of Molecular Pharmacology and Discovery Informatics, Aachen, Germany (A.K., G.B.)

Received September 6, 2010; accepted December 29, 2010

ABSTRACT

P2X2 receptors are members of the ATP-gated P2X family of cation channels, and they participate in neurotransmission in sympathetic ganglia and interneurons. Here, we identified 7,7'-(carbonylbis(imino-3,1-phenylenecarbonylimino-3,1-(4-methylphenylene)carbonylimino))bis(1-methoxy-naphthalene-3,6-disulfonic acid) tetrasodium salt (NF770) as a nanomolar-potent competitive P2X2 receptor antagonist within a series of 139 suramin derivatives. Three structural determinants contributed to the inhibition of P2X2 receptors by NF770: 1) a “large urea” structure with two symmetric phenylenecarbonylimino groups; 2) attachment of the naphthalene moiety in position 7,7'; and 3) the specific position of two sulfonic acid groups (3,3'; 6,6') and of one methoxy group (1,1') at the naphthalene moiety. This structure-activity relationship was interpreted using a rat P2X2 homology model based on the crystal structure of the

closed zebrafish P2X4 receptor. Docking of the suramin derivatives into the modeled ATP-binding pocket provides a uniform explanation for the observed differences in inhibitory potencies. Changes in the chemical structure that increase the inhibitory potency of the suramin derivatives improved the spatial orientation within the ATP-binding pocket to allow for stronger polar interactions of functional groups with Gly72, Glu167, or Arg290. Gly72 is responsible for the orientation of the methoxy group close to Arg290 or Glu167. Combined mutational and functional analysis confirmed that residues Gly72 and Glu167 are as important for ATP binding as Arg290, the ATP-binding role of which has been shown in previous studies. The *in silico* prediction of Gly72 and Glu167 as ATP-binding residues strongly supports the validity of our homology docking.

Introduction

P2X receptors, a family of ion channels that are gated by extracellular ATP, are homotrimers and heterotrimers (Nicke et al., 1998; Aschrafi et al., 2004) assembled from a repertoire of seven homologous subunits, P2X1 to P2X7 (Burnstock, 2004). P2X receptors are expressed on the surface of a large variety of excitable and nonexcitable cell types and are involved in numerous processes, including sensory neurotransmission, platelet aggregation, smooth muscle contraction, immune responses, and inflammation (Finger et al., 2005; Gevertz et al., 2006; Burnstock, 2008; Jarvis and Khakh, 2009; Surprenant and North, 2009). There is strong evidence

that at least four P2X receptor subtypes play a role in nociception, including homomeric P2X3, P2X4, and P2X7 receptors and the heteromeric P2X2/3 receptor (Burnstock, 2008; Surprenant and North, 2009).

Several P2X receptor antagonists have been developed to target pain and inflammation. 5-[[[(3-Phenoxyphenyl)methyl][(1S)-1,2,3,4-tetrahydro-1-naphthalenyl]amino]carbonyl]-1,2,4-benzenetricarboxylic acid sodium salt hydrate (A-317491), a selective dual inhibitor of P2X3 and P2X2/3 receptors, has strong antinociceptive effects in rodents (Jarvis et al., 2002), but it has not been developed further because of its poor distribution into the central nervous system (Gevertz et al., 2006). Selective dual inhibition of P2X3 and P2X2/3 receptors has also been achieved by the diaminopyrimidine derivatives 5-(2-isopropyl-4,5-dimethoxy-benzyl)-pyrimidine-2,4-diamine (RO-3), 5-(5-iodo-2-isopropyl-4-methoxy-phenoxy)-pyrimidine-2,4-diamine (RO-4), and RO-51 (Jahangir et al., 2009; Jarvis and Khakh, 2009; Gevertz et al., 2010). Among these, RO-3 and RO-4 (recently redesignated AF-353) distribute well into tissues, including the cen-

This work was supported by the Deutsche Forschungsgemeinschaft [Grants Schm 536/8-1/2 (to G.S.), Schm 536/8-2 (to R.H.), Graduiertenkolleg GRK677 (to M.U.K.)].

¹ C.W. and C.R., contributed equally to this work.

Article, publication date, and citation information can be found at <http://molpharm.aspetjournals.org>.

doi:10.1124/mol.110.068700.

[S] The online version of this article (available at <http://molpharm.aspetjournals.org>) contains supplemental material.

tral nervous system, and exert beneficial effects in rodent models of pain and models of bladder function (Gever et al., 2006, 2010; Jarvis, 2010). 1-methyl-3-phenyl-1*H*-thieno[2,3-*c*]pyrazole-5-carboxylic acid [(*R*)-2-(4-acetyl-piperazin-1-yl)-1-methyl-ethyl]-amide (RO-85), the first orally bioavailable drug-like P2X₃ receptor antagonist, is selective for P2X₃ receptors over P2X_{2/3} and other P2X receptor subtypes. RO-85 inhibits rat and human P2X₃ receptors with pIC₅₀ values of 7.5 and 6.4, respectively, and is only weakly potent (pIC₅₀ < 5) at non-P2X₃ receptor subtypes, including the human P2X_{2/3} receptor (Brotherton-Pleiss et al., 2010). The newly developed P2X₇ receptor-selective antagonists (adamantan-1-ylmethyl)-5-[(3*R*-amino-pyrrolidin-1-yl)methyl]-2-chloro-benzamide (GSK314181A), *N*-(1-[[[cyanoimino](5-quinolinylamino)methyl]amino]-2,2-dimethylpropyl)-2-(3,4-dimethoxyphenyl)acetamide (A-740003), 3-[[5-(2,3-dichlorophenyl)-1*H*-tetrazol-1-yl]methyl]pyridine hydrochloride (A-438079), 1-(2,3-dichlorophenyl)-*N*-[2-(pyridin-2-yloxy)benzyl]-1*H*-tetrazol-5-amine (A-839977), and 2-cyano-1-[(1*S*)-1-phenylethyl]-3-quinolin-5-ylguanidine (A-804598) also have analgesic effects in rodent models of pain (for review, see Jarvis, 2010).

The reduced nociceptive signaling seen in P2X₂ knockout mice during the persistent phase of the formalin model of pain seems to result from reduced signaling through heteromeric P2X_{2/3} channels rather than from homomeric P2X₂ receptors (Cockayne et al., 2005). In several acute pain models, however, P2X₂-containing receptors (homomeric P2X₂ and heteromeric P2X_{2/3} receptors) are not critical for acute nociceptive responses (Cockayne et al., 2005). By contrast, homomeric P2X₂ receptors facilitate excitatory transmission onto interneurons (Khakh et al., 2003) and play pivotal roles in the mediation of neuronal ventilatory responses (Rong et al., 2003) and in sympathetic autonomous neurotransmission (Cockayne et al., 2005). P2X_{2/3} heteromeric receptors are also involved in the transmission of sensory information from taste buds, but they are less important than P2X₃ receptors in this pathway (Finger et al., 2005). Pharmacological experiments evaluating the role of homomeric P2X₂ receptors in these processes are impeded by the lack of selective agonists and potent antagonists (Burnstock, 2008; Jarvis and Khakh, 2009). Current P2X receptor antagonists are nonselective and have, at best, micromolar potencies for P2X₂ receptors

(Gever et al., 2006; Jarvis and Khakh, 2009). PPADS, for instance, blocks homomeric P2X₁, P2X₂, and P2X₃ receptors with a similar IC₅₀ of ~1 μM (Gever et al., 2006; Jarvis and Khakh, 2009). TNP-ATP blocks P2X₁, P2X_{2/3}, and P2X₃ receptors with nanomolar potency, but it is 1000-fold less potent in blocking homomeric P2X₂ receptors (Gever et al., 2006; Jarvis and Khakh, 2009). We have previously identified the suramin derivatives 4,4',4'',4'''-(carbonylbis(imino-5,1,3-benzenetriyl-bis(carbonylimino)))tetrakisbenzene-1,3-disulfonic acid-octasodium salt (NF449) and 4,4',4'',4'''-(carbonylbis(imino-5,1,3-benzenetriyl-bis(carbonylimino)))tetrakisbenzenesulfonic acid (NF110) as potent antagonists of P2X₁ and P2X₃ receptors, respectively (Kassack et al., 2004; Rettinger et al., 2005; Hausmann et al., 2006). Suramin itself nonselectively inhibits P2X₂ receptors with a potency similar to that of PPADS or TNP-ATP (Trujillo et al., 2006; Jarvis and Khakh, 2009). Consequently, we screened a series of 139 suramin derivatives and identified 7,7'-(carbonylbis(imino-3,1-phenylenecarbonylimino-3,1-(4-methyl-phenylene)carbonylimino))bis(1-methoxy-naphthalene-3,6-disulfonic acid) tetrasodium salt (NF770) as a P2X₂ receptor antagonist with nanomolar potency and selectivity over P2X₁, P2X₄, and P2X₇ receptors.

The 3.0-Å resolution X-ray structure of the closed-state zebrafish (zf) P2X₄ receptor (Kawate et al., 2009) enables homology modeling of other P2X receptor family members for rational ligand design (Jarvis, 2010) and facilitated mutagenesis-based studies of structural rearrangements that accompany channel opening (Cao et al., 2009; Keceli and Kubo, 2009; Jiang et al., 2010; Kracun et al., 2010). For a molecular interpretation of the observed structure-activity relationships, we generated a closed-state homology model for rat P2X₂ (rP2X₂) using zfpP2X_{4.1} structure (Kawate et al., 2009) as template and performed in silico docking experiments that resulted in the identification of the molecular determinants of P2X₂ antagonism and two novel amino acid residues important for ligand binding.

Materials and Methods

Chemicals. A diverse library of suramin derivatives available from previous studies was synthesized according to published methods (Kassack et al., 2004; Ullmann et al., 2005). The chemical struc-

ABBREVIATIONS: A-317491, 5-[[[(3-Phenoxyphenyl)methyl][(1*S*)-1,2,3,4-tetrahydro-1-naphthalenyl]amino]carbonyl]-1,2,4-benzenetricarboxylic acid sodium salt hydrate; RO-3, 5-(2-isopropyl-4,5-dimethoxy-benzyl)-pyrimidine-2,4-diamine; RO-4, 5-(5-iodo-2-isopropyl-4-methoxy-phenoxy)-pyrimidine-2,4-diamine; GSK314181A, (adamantan-1-ylmethyl)-5-[(3*R*-amino-pyrrolidin-1-yl)methyl]-2-chloro-benzamide; A-740003, *N*-(1-[[[cyanoimino](5-quinolinylamino)methyl]amino]-2,2-dimethylpropyl)-2-(3,4-dimethoxyphenyl)acetamide; A-804598, 2-cyano-1-[(1*S*)-1-phenylethyl]-3-quinolin-5-ylguanidine; PPADS, pyridoxalphosphate-6-azophenyl-2',4'-disulfonic acid; TNP-ATP, 2',3',3'-O-(2,4,6-trinitrophenyl)-ATP; r, rat; zf, zebrafish; ORi, oocyte Ringer solution; αβ-meATP, αβ-methylene-ATP; TEVC, two-electrode voltage-clamp; PAGE, polyacrylamide gel electrophoresis; NF449, 4,4',4'',4'''-(carbonylbis(imino-5,1,3-benzenetriyl-bis(carbonylimino)))tetrakisbenzene-1,3-disulfonic acid-octasodium salt; NF110, 4,4',4'',4'''-(carbonylbis(imino-5,1,3-benzenetriyl-bis(carbonylimino)))tetrakisbenzenesulfonic acid; NF770, 7,7'-(carbonylbis(imino-3,1-phenylenecarbonylimino-3,1-(4-methyl-phenylene)carbonylimino))bis(1-methoxy-naphthalene-3,6-disulfonic acid) tetrasodium salt; NF742, 8,8'-(carbonylbis(imino-3,1-phenylenecarbonylimino-3,1-(4-methyl-phenylene)carbonylimino))bis(1-methoxy-naphthalene-3,6-disulfonic acid) tetrasodium salt; NF769, 7,7'-(carbonylbis(imino-3,1-(4-methyl-phenylene)carbonylimino))bis(1-methoxy-naphthalene-3,6-disulfonic acid) tetrasodium salt; NF778, 6,6'-(carbonylbis(imino-3,1-phenylenecarbonylimino-3,1-(4-methyl-phenylene)carbonylimino))bis(1-methoxy-naphthalene-3,5-disulfonic acid) tetrasodium salt.; NF127, 8,8'-(carbonylbis(imino-3,1-phenylenecarbonylimino-3,1-(4-ethylphenylene)carbonylimino))bis(naphthalene-1,3,5-trisulfonic acid) hexasodium salt; NF739, 8,8'-(carbonylbis(imino-3,1-(4-methylphenylene)carbonylimino))bis(1-methoxynaphthalene-3,6-disulfonic acid) tetrasodium salt; NF776, 6,6'-(carbonylbis(imino-3,1-(4-methylphenylene)carbonylimino))bis(1-methoxynaphthalene-3,5-disulfonic acid) tetrasodium salt; 2D, two-dimensional; NF279, 8,8'-[carbonylbis(imino-4,1-phenylenecarbonylimino-4,1-phenylenecarbonylimino)]bis-1,3,5-naphthalenetrisulfonic acid hexasodium salt; TM, transmembrane; RO-85, 1-methyl-3-phenyl-1*H*-thieno[2,3-*c*]pyrazole-5-carboxylic acid [(*R*)-2-(4-acetyl-piperazin-1-yl)-1-methyl-ethyl]-amide; A-839977, 1-(2,3-dichlorophenyl)-*N*-[2-(pyridin-2-yloxy)benzyl]-1*H*-tetrazol-5-amine; NF708, 3,3'-(carbonylbis(imino-3,1-phenylene)carbonylimino))bis(benzenephosphonic acid) tetrasodium salt; NF739, 8,8'-(carbonylbis(imino-3,1-(4-methylphenylene)carbonylimino))bis(1-methoxynaphthalene-3,6-disulfonic acid)tetrasodium salt.

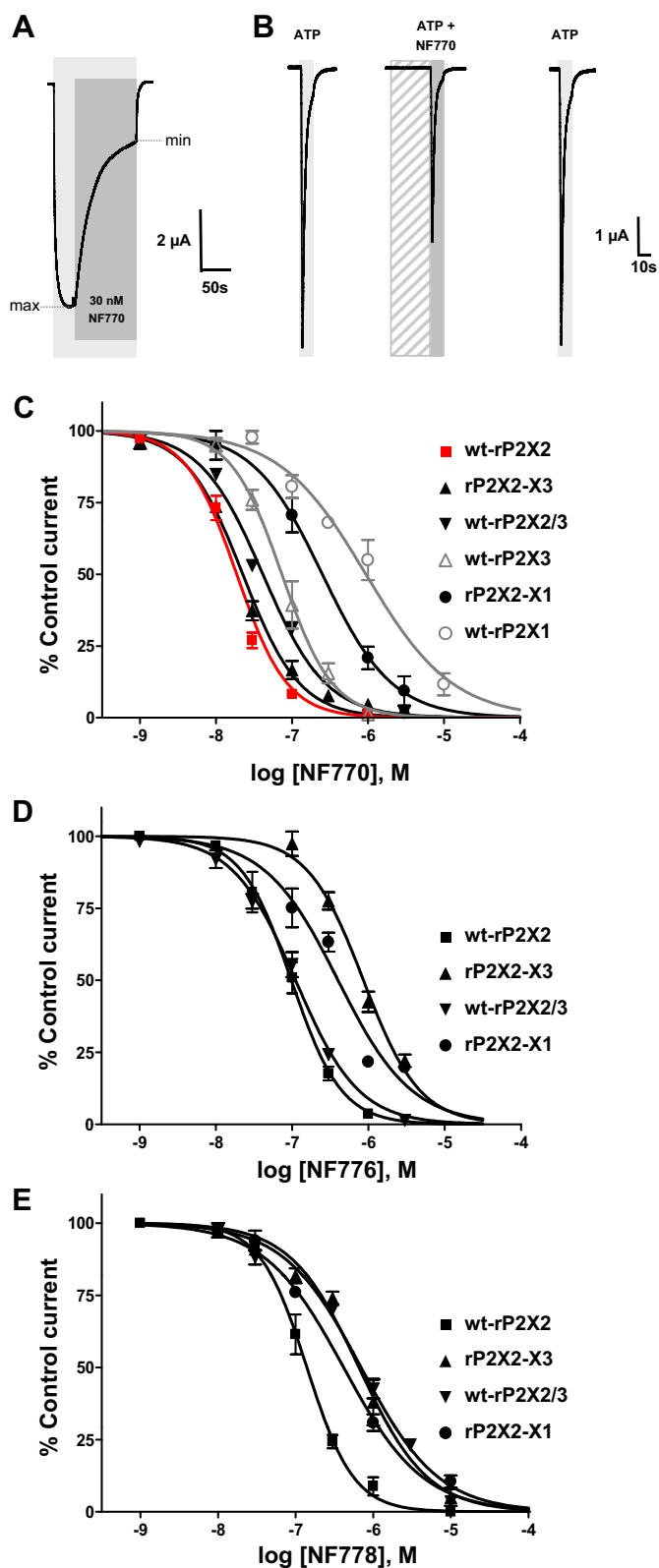


Fig. 1. Potencies of NF770, NF776, and NF778 at different rP2X receptor isoforms. **A**, steady-state protocol for the assessment of the inhibitory potency of NF770 from stationary current measurements. A representative original current trace is shown. After a maximal stationary current (max) was elicited with 10 μ M ATP (light gray), 30 nM NF770 was coapplied with 10 μ M ATP (dark gray). The current declined until a new steady state was reached, designated the minimum current (min), indicating that inhibition by NF770 was fully developed. The application of ATP and NF770 was then terminated. The extent of inhibition was

judged from the ratio of the maximal and minimal stationary current in the absence and presence of NF770, respectively. **B**, traces representing the protocol for the assessment of the inhibitory potency of NF770 from peak current measurements. Representative original current traces are shown. rP2X1 receptor-expressing oocytes were repetitively activated with 1 μ M ATP (light gray) at 1-min intervals. Between two control measurements, the oocytes were pre-equilibrated with 300 nM NF770 for 30 s (hatched gray) and then challenged with 1 μ M ATP in the continued presence of NF770 (dark gray). The extent of inhibition was judged from the reduction of the peak current amplitude compared with the two flanking control measurements.

C to **E**, using the appropriate steady-state or peak-current protocol, concentration-inhibition curves were generated in the presence of incrementally larger concentrations of NF770 (**C**), NF776 (**D**), and NF778 (**E**). For convenience, all IC_{50} values of NF770, NF776, and NF778 are summarized in Table 1, and the chemical structures are shown in Table 2.

Two-Electrode Voltage-Clamp Electrophysiology. One to three days after cRNA injection, current responses were evoked with ATP or $\alpha\beta$ -meATP at ambient temperature (21–24°C) in the absence or presence of suramin derivatives and recorded with conventional two-electrode voltage-clamp (TEVC) with a Turbo TEC-05 amplifier (NPI Electronic GmbH, Tamm, Germany) at a holding potential of –60 mV, as described previously (Hausmann et al., 2006). On the day of the experiment, agonists and suramin derivatives were diluted from the frozen aqueous stock solutions. Oocytes were continuously perfused by gravity flow (5–10 ml/min) in a small flow-through chamber (volume, ~10 μ l) with a nominally calcium-free ORi solution (designated Mg-ORi) in which $CaCl_2$ was replaced with equimolar $MgCl_2$ to avoid a contribution of endogenous Ca^{2+} -dependent chloride channels to the agonist response. To record rP2X7 receptor-mediated currents, a bathing solution consisting of 94 mM NaCl, 1 mM KCl, 0.1 mM flufenamic acid, and 10 mM HEPES-NaOH, pH 7.4, was used (Hausmann et al., 2006; Becker et al., 2008). Switching between bath solutions was controlled by a set of computer-operated magnetic valves controlled by the CellWorks E 5.1 software (NPI Electronic GmbH). When analyzing the inhibitory effects, the following agonist concentrations were used: 100 μ M ATP for rP2X7, 10 μ M ATP for rP2X2 and rP2X4, 1 μ M ATP for rP2X1 and rP2X3, 10 nM ATP for rP2X2-X1 and rP2X2-X3 chimeras, and 1 μ M $\alpha\beta$ -meATP for rP2X2/3 (Hausmann et al., 2006). The application of agonists and antagonists was tailored to fit the specific experimental needs of each P2X receptor based on the presence or absence

judged from the ratio of the maximal and minimal stationary current in the absence and presence of NF770, respectively. **B**, traces representing the protocol for the assessment of the inhibitory potency of NF770 from peak current measurements. Representative original current traces are shown. rP2X1 receptor-expressing oocytes were repetitively activated with 1 μ M ATP (light gray) at 1-min intervals. Between two control measurements, the oocytes were pre-equilibrated with 300 nM NF770 for 30 s (hatched gray) and then challenged with 1 μ M ATP in the continued presence of NF770 (dark gray). The extent of inhibition was judged from the reduction of the peak current amplitude compared with the two flanking control measurements.

of desensitization, as reported previously (Hausmann et al., 2006). Representative current traces from the nondesensitizing rP2X2 receptor and the fast-desensitizing rP2X1 receptor are shown in Fig. 1.

Protein Labeling, Purification, and PAGE. cRNA-injected oocytes were metabolically labeled by overnight incubation with [35 S]methionine. Immediately before protein extraction, the oocytes were additionally surface-labeled with Cy5 *N*-hydroxysuccinimide ester, an amine-reactive, membrane-impermeant fluorescent dye, as described previously (Becker et al., 2008). His-tagged proteins were purified by nickel-nitrilotriacetic acid agarose (QIAGEN, Valencia, CA) chromatography from digitonin [1% (w/v)] extracts and analyzed with the use of blue native PAGE, as described previously (Nicke et al., 1998; Aschrafi et al., 2004). The migration positions of P2X2 dimers and monomers were determined by coanalyzing the partially denatured P2X2 receptor. This was achieved by treating the samples for 1 h at 37°C with 0.1% (w/v) SDS or a combination of 0.1% (w/v) SDS and 100 mM dithiothreitol before blue native PAGE.

For SDS-urea-PAGE, proteins were denatured by incubation with a reducing SDS sample buffer for 15 min at 56°C and electrophoresed in parallel with 14 C-labeled molecular weight markers (Rainbow; GE Healthcare, Chalfont St. Giles, Buckinghamshire, UK) on SDS-urea gels with 10% acrylamide. After electrophoresis, gels were scanned wet with a fluorescence scanner (Typhoon; GE Healthcare) to visualize the fluorescently labeled plasma membrane-bound proteins and then dried and exposed to a phosphor screen for subsequent analysis using a Storm 820 PhosphorImager (GE Healthcare) to detect 35 S incorporation. Figures were prepared with ImageQuant TL (ver. 2005; GE Healthcare) for contrast adjustments and Photoshop CS 4 (Adobe Systems, Mountain View, CA) for level adjustment and cropping.

Data Analysis. Data were plotted and fitted using Prism (ver. 5; GraphPad Software, Inc., San Diego, CA). Agonist concentration-response values were generated by normalizing the current amplitudes to the control response induced by a supermaximally effective ATP concentration of 1 mM. Agonist concentration-response curves and EC₅₀ values were obtained by iteratively fitting the Hill equation to the normalized data points from 5 to 11 oocytes: $I/I_{\max} = 1/(1 + ([EC_{50}/A])^{n_H})$, where I is the current evoked by agonist concentration A , I_{\max} is the maximal current response, and n_H is the Hill coefficient.

Antagonist concentration-response values were generated by normalizing the ATP-induced current amplitudes in the presence of the antagonist to the control response in the absence of the antagonist. Concentration-inhibition curves and IC₅₀ values were derived from the nonlinear least-squares fit of the pooled data points: $I_{\text{Ant}}/I_{\max} = 1/(1 + ([Ant]/IC_{50})^{n_H})$, where I_{\max} is the control response in the absence of antagonist (Ant), I_{Ant} is the current response at the respective antagonist concentration, and IC₅₀ is the antagonist concentration that causes 50% inhibition of the current elicited by a given agonist concentration.

EC₅₀ and IC₅₀ values are presented as the geometric means and their 95% confidence intervals. Mean current amplitudes, Hill slopes, and other values are presented as arithmetic means \pm S.E.M. Error bars were omitted in the figures when they were smaller than the symbols used.

Homology Model of the rP2X2. We used the standard modeling techniques implemented in MOE2008.10 (Molecular Operating Environment 2008; Chemical Computing Group, Montreal, QC, Canada) to generate a homology model of the rP2X2 receptor based on the X-ray structure of zP2X4 (Kawate et al., 2009). Protein Data Bank entry 3H9V, which is believed to represent the closed state of the channel, was used as a template. The sequence of rP2X2 was retrieved from accession number P49653 of the UniProtKB database. Sequence alignment between the template and the model sequence was performed using a modified version of the alignment algorithm originally introduced by Needleman and Wunsch (1970). In this approach, alignments are computed by optimizing a function based on residue similarity scores. The function uses the amino acid substitution matrix BLOSUM62 (Henikoff and Henikoff, 1992) and gap penalties; it was constrained, in this case, by the 10 known conserved extracellular cysteine

residues, which were adjusted and fixed manually. The presented homology model is based on the best scoring of 25 generated intermediate models and the overall structural quality confirmed by a Ramachandran plot. The intermediate homology models were refined with the Amber89 force field (Summa and Levitt, 2007) using a fine gradient, which was terminated when the root-mean-square was <1 Å. The electrostatic solvation energy was used to score the 25 models; it was calculated using a generalized born/volume integral method (Labute, 2008). The protonation of the final model was done using the Protonate3D algorithm followed by minimization with a root-mean-square of 0.5 Å (Labute, 2009). This homology model was used for the docking procedure (Fig. 3). The lowest energy conformations of the suramin derivatives [8,8'-(carbonylbis(imino-3,1-phenylenecarbonylimino-3,1-(4-methyl-phenylene)carbonylimino))bis(1-methoxynaphthalene-3,6-disulfonic acid) tetrasodium salt (NF742), 7,7'-(carbonylbis(imino-3,1-(4-methyl-phenylene)carbonylimino))bis(1-methoxynaphthalene-3,6-disulfonic acid) tetrasodium salt (NF769), NF770, and 6,6'-(carbonylbis(imino-3,1-phenylenecarbonylimino-3,1-(4-methyl-phenylene)carbonylimino))bis(1-methoxynaphthalene-3,5-disulfonic acid) tetrasodium salt (NF778)] were deprotonated to sulfonates, as they exist at physiological pH. The receptor model was kept rigid during the docking computation, whereas the suramin derivatives were allowed to remain flexible, permitting possible bond rotations.

Results

Three (of 139) Suramin Analogs Exhibit Nanomolar Potency at the rP2X2 Receptor. At 10 μ M ATP, suramin inhibited the oocyte-expressed rP2X2 receptor with an IC₅₀ value of 0.49 μ M. This value is at the bottom of the range of published IC₅₀ values (1–34 μ M; Gevert et al., 2006). In contrast, our EC₅₀ value (95% confidence interval) for ATP of 21.8 (17.4–23.2) μ M was in the range reported by others (Jiang et al., 2010). The unexpectedly potent inhibition of the rP2X2 receptor by suramin prompted us to screen an available library of 139 suramin derivatives synthesized according to methods published previously (Kassack et al., 2004; Ullmann et al., 2005). To accelerate TEVC screening, we arranged 1 μ M aqueous solutions of 139 suramin derivatives in two sets of matrices, A and B, composed of 81 and 58 derivatives, respectively. Equal aliquots from each horizontal row were combined to yield row mixtures of nine or six to seven suramin derivatives. Likewise, equal aliquots from each vertical column were combined to yield column mixtures of nine or, in one case, four suramin derivatives. Accordingly, each compound was present in two mixtures: one row and one column mixture. With a total of 34 TEVC measurements representing 18 rows and 16 columns, we could identify four row mixtures and three column mixtures that inhibited the rP2X2 receptor-mediated currents by $>75\%$. By determining the intersection of active row and column mixtures, seven putatively active suramin derivatives were identified: 8,8'-(carbonylbis(imino-3,1-phenylenecarbonylimino-3,1-(4-ethylphenylene)-carbonylimino))bis(naphthalene-1,3,5-trisulfonic acid) hexasodium salt (NF127), 3,3'-(carbonylbis(imino-3,1-phenylene)carbonylimino))bis(benzenephosphonic acid) tetrasodium salt (NF708), 8,8'-(carbonylbis(imino-3,1-(4-methylphenylene)carbonylimino))bis(1-methoxynaphthalene-3,6-disulfonic acid) tetrasodium salt (NF710), 8,8'-(carbonylbis(imino-3,1-(4-methylphenylene)carbonylimino))bis(1-methoxynaphthalene-3,6-disulfonic acid) tetrasodium salt (NF739), NF770, 6,6'-(carbonylbis(imino-3,1-(4-methylphenylene)carbonylimino))bis(1-methoxynaphthalene-3,5-disulfonic acid) tetrasodium salt (NF776), and NF778. Individual testing showed that at 1 μ M, NF708, NF710, NF127, and NF739

inhibited the ATP-gated rP2X2 receptor currents by 18, 7, 39, and 14%, respectively, and they were not tested further at the other P2X receptor isoforms. In contrast, NF770, NF776, and NF778, at 1 μ M each, inhibited the ATP-gated rP2X2 receptor currents by 84 to 96% and were characterized in detail.

Concentration-response Analysis of NF770, NF776, and NF778 at Different P2X Receptor Subtypes. To determine the P2X receptor subtype selectivity of the three most potent rP2X2 receptor-blocking suramin derivatives (NF770, NF776, and NF778), concentration-response curves were generated for the rP2X1, rP2X2, rP2X2/3, rP2X3, rP2X4, and rP2X7 receptors (Fig. 1, C–E). The P2X5 receptor was not studied because in humans, the P2X5 subunit occurs predominantly as an assembly-deficient natural deletion mutant that lacks much of the TM2 and pre-TM2 regions as a result of the splicing out of exon 10 (Duckwitz et al., 2006). The P2X6 receptor was also omitted because P2X6 does not form functional homomeric channels under most circumstances (Gever et al., 2006). ATP elicited nondesensitizing currents in wt-rP2X2 and wt-rP2X2/3 receptors. This allowed for the steady-state analysis of drug-induced current inhibition as a visible decline of the current amplitude to a new plateau (see current traces in Fig. 1A). In contrast, wt-rP2X1 and wt-rP2X3 receptors desensitized rapidly in the continued presence of agonist (see current traces in Fig. 1B). If agonist and antagonist bind to the same receptor with different rate constants, the current transient is too short to allow a binding equilibrium to be reached between the coapplied compounds (Hausmann et al., 2006). To assess the inhibition of P2X1 and P2X3 receptors under steady-state conditions, nondesensitizing rP2X2-X1 and rP2X2-X3 receptor chimeras were used, in which the N-terminal tail, including the first transmembrane domain, are replaced by the complementary portion of the rP2X2 subunit (Hausmann et al., 2006). Because the ligand-binding ectodomain originates entirely from the rP2X1 or the rP2X3 subunit, these chimeras can be reliably used as nondesensitizing substitutes of wt-rP2X1 and rP2X3 receptors. Although ATP served as an agonist for all the above receptors, the nondesensitizing heteromeric rP2X2/3 receptor was selectively activated by 1 μ M α β -meATP to avoid activation of the coexpressed homomeric rP2X2 receptor, which responds to ATP but virtually not to α β -meATP (Gever et al., 2006).

Concentration-inhibition curves and IC₅₀ values were derived from nonlinear least-squares fits of the Hill equation to

the pooled data points. The following rank order of potencies was determined for NF770 (Fig. 1C, Table 1): wt-rP2X2 \geq rP2X2-X3 > wt-rP2X2/3 > wt-rP2X3 > rP2X2-X1 > wt-rP2X1 \gg wt-rP2X4, wt-rP2X7. A similar rank order was obtained for NF776 and NF778, except that the positions of rP2X1 and rP2X3 were reversed (Fig. 1, D and E; Table 1). All three suramin derivatives were almost ineffective in blocking rP2X4 or rP2X7 receptor-mediated currents (<10% inhibition at 10 μ M for either suramin derivative; data not shown).

NF770 Inhibits the rP2X2 Receptor Competitively.

To delineate whether NF770 acts as a competitive antagonist of the P2X2 receptor, ATP concentration-response curves were established in the absence and presence of NF770. Representative current traces recorded at distinct concentrations of NF770 are shown in Fig. 2A. In this experimental series, ATP-activated rP2X2 receptor-mediated inward currents with an EC₅₀ value of 20.7 μ M. Increasing concentrations of NF770 progressively shifted the ATP concentration-response curves parallel to the right without changing the maximal response (Fig. 2B). Linear regression analysis of Schild plot data (Fig. 2C) yielded a correlation coefficient of 0.996, a slope of 0.74 ± 0.03 , and an abscissa intercept of -6.96 , corresponding to a pA₂ value of 6.96. All together, these data strongly indicate that NF770 and ATP interact competitively at the rP2X2 receptor.

Structure-Activity Relationships of Suramin Derivatives as P2X2 Receptor Antagonists. To identify the structural determinants of P2X2 receptor inhibition, we established concentration-response relationships for compounds that are more closely related to either suramin (compound 2) or to NF770 (compound 15) in terms of the number of sulfonic acid groups or the presence of a methoxy group, respectively. The chemical structures of these compounds and their IC₅₀ values at the rP2X2 receptor are shown in Table 2. Large urea derivatives contained two symmetric phenylenecarbonylimino groups linking the urea backbone with the naphthalene moieties (Table 2, compounds 1–3 and 13–16). Small urea derivatives contained only one symmetric phenylenecarbonylimino group between the urea backbone and the naphthalene moieties (Table 2, compounds 4–12).

Replacing the methyl substituent of the phenylene ring of suramin with hydrogen (compound 1) or ethyl (compound 3) had virtually no effect on the inhibitory potency (IC₅₀, 0.28–0.49 μ M). The corresponding small urea derivatives (i.e., compounds 4–6) were 30- to 46-fold less potent in inhibiting the rP2X2 receptor (IC₅₀, 9.9–14.4 μ M). The potency declined further

TABLE 1

Survey of the potencies of NF770, NF776, and NF778 at various recombinant P2X receptors

IC₅₀ values represent data from five to seven separate experiments. "Normalized" means normalized to the following IC₅₀ values for rP2X2 receptor inhibition: 19 nM NF770, 97 nM NF776, and 140 nM NF778.

	NF770			NF776			NF778		
	–log IC ₅₀ (95% CI)	IC ₅₀	Normalized IC ₅₀	–log IC ₅₀ (95% CI)	IC ₅₀	Normalized IC ₅₀	–log IC ₅₀ (95% CI)	IC ₅₀	Normalized IC ₅₀
	<i>nM</i>			<i>nM</i>			<i>nM</i>		
wt-rP2X1	6.03 (6.20–5.86)	939	49.4	N.D.	N.D.		N.D.	N.D.	
rP2X2-X1	6.60 (6.76–6.44)	251	13.2	6.40 (6.52–6.27)	400	4.1	6.38 (6.47–6.29)	415	3.0
wt-rP2X2	7.73 (7.79–7.67)	19	1	7.01 (7.08–6.94)	97	1	6.86 (6.92–6.79)	140	1
wt-rP2X3	7.13 (7.21–7.05)	74	3.9	N.D.	N.D.		N.D. ^e	N.D.	
rP2X2-X3	7.65 (7.69–7.60)	23	1.2	6.07 (6.14–5.99)	861	8.9	6.18 (6.31–6.06)	655	4.7
wt-P2X2/3	7.38 (7.44–7.33)	41	2.2	6.96 (7.02–6.89)	111	1.1	6.16 (6.23–6.08)	698	5.0
wt-rP2X4	> 5	> 10,000		> 5	> 10,000		> 5	> 10,000	
wt-rP2X7	> 5	> 10,000		> 5	> 10,000		> 5	> 10,000	

95% CI, 95% confidence interval; N.D., not determined.

when the position of one of the sulfonic acid groups was changed from the *para* to the *meta* position relative to the amino group (compare compounds 5 and 7). In contrast, replacement of the sulfonic acid group in position 1 by a methoxy group in the small urea backbone increased the inhibitory potency ~ 4 -fold when the positions of the two remaining sulfonic acid groups were left unchanged (compare compounds 7 and 8) and ~ 2 -fold when the two remaining sulfonic acid groups were differently positioned (compare compounds 7 and 9).

An increase in the inhibitory potency of the trisulfonic acid derivatives also occurred when the position of the naphthalene moiety relative to the amino group was changed from position 8,8' (α -aminonaphthalene, compounds 4–7) to position 7,7' (β -aminonaphthalene, compound 10). Combining the replacement of one sulfonic acid group by a methoxy group and replacing the α -aminonaphthalene by a β -aminonaphthalene [corresponding to position 7,7' in compound 15 (NF770) and to position 6,6' in compound 12 (NF776)] increased the inhibitory potency further (compare compounds 10 and 11 or 12). The resulting compound, NF776 (compound 12), was the most potent rP2X2 receptor blocker in this series of small urea derivatives.

Next, we examined whether similar beneficial effects could also be realized in the context of large urea derivatives. We

observed a ~ 34 -fold increase of the inhibitory potency of the 8,8'-aminonaphthalene derivatives by changing the position of the methoxy group at the naphthalene moiety from position 1 to 3 (compare compounds 13 and 14). An even larger (>1000 -fold) increase occurred when the α -aminonaphthalene moiety was replaced by a β -aminonaphthalene [from the 8,8' (compound 13) to the 7,7' position (compound 15)], thus yielding the most potent rP2X2 receptor-blocking suramin derivative in this study, NF770. The solely available α -aminonaphthalene derivative with positionally different sulfonic acid and methoxy groups, NF778 (compound 16), was 7-fold less potent than NF770 (compound 15), again indicating the importance of the position of the methoxy group.

Molecular Docking of Suramin Derivatives on a Homology-Modeled rP2X2 Receptor. The above results identified three structural determinants of suramin derivatives that contribute to efficient P2X2 receptor inhibition: 1) a “large urea” structure with two symmetric phenylencarbonylimino groups linking the urea backbone with the naphthalene moiety, 2) substitution of one of the three sulfonic acid groups by a methoxy group, and 3) using a β -aminonaphthalene moiety rather than a α -aminonaphthalene. To assign these chemical structure determinants to molecular features of the rP2X2 ATP-binding pocket, we generated a homology model of the rP2X2 receptor

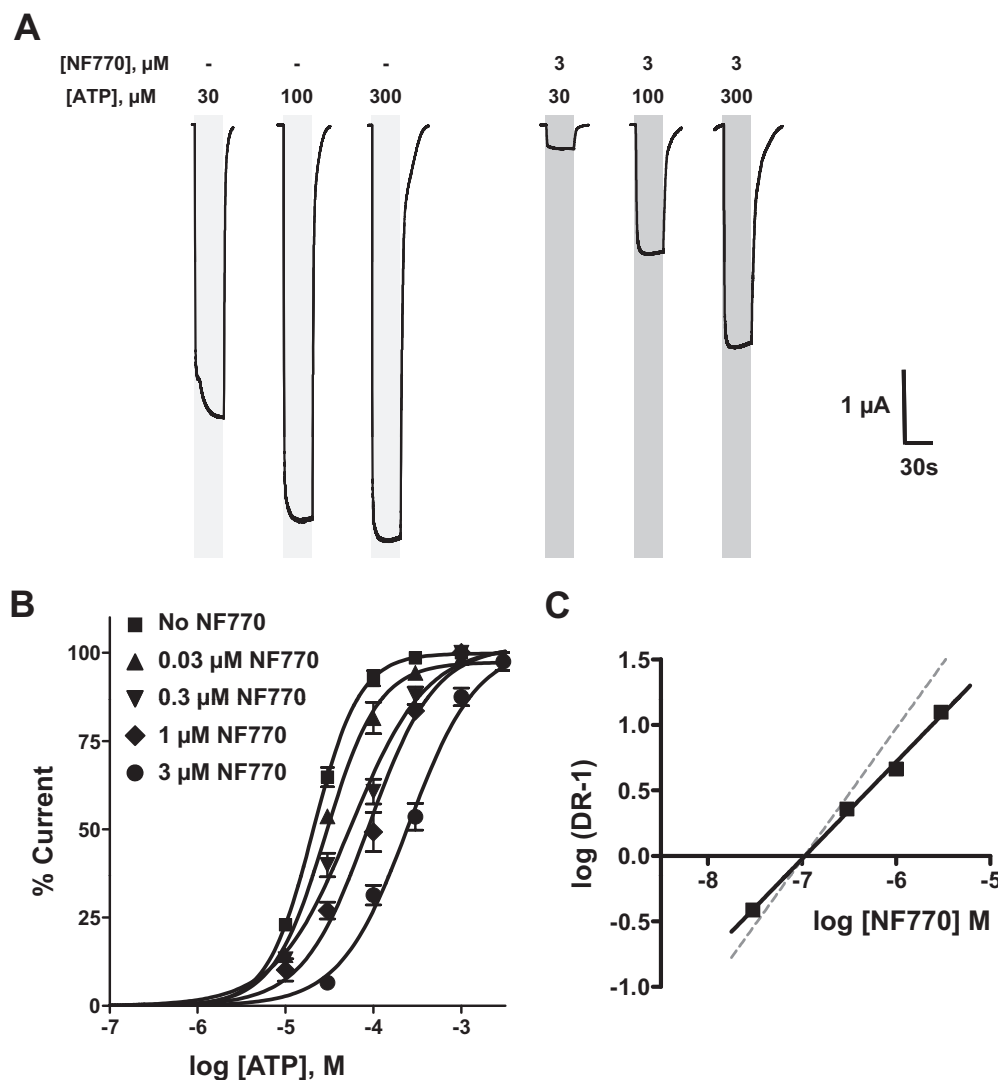


Fig. 2. Assessment of the mechanism of NF770-induced inhibition of the rP2X2 receptor. **A**, representative original current traces are shown. Oocytes expressing rP2X2 receptors were repetitively activated with indicated increasing concentrations of ATP in the absence (light gray) or the presence of 3 μM NF770 (dark gray), respectively. **B**, ATP concentration-response curves were established by stimulating oocytes expressing the rP2X2 receptor with incrementally larger concentrations of ATP in the absence of NF770 [■, EC_{50} , 20.7 μM (95% confidence interval, 18.9–22.7); n_H , 1.7 ± 0.1 , $n = 11$] or the presence of 30 nM NF770 [▲, EC_{50} , 28.7 μM (23.2–35.6); n_H , 1.4 ± 0.2 , $n = 5$], 300 nM NF770 [▼, EC_{50} , 67.9 μM (47.4–97.1); n_H , 0.9 ± 0.1 , $n = 6$], 1 μM NF770 [◆, EC_{50} , 116.1 μM (78.1–172.4); n_H , 1.0 ± 0.1 , $n = 6$] and 3 μM NF770 [●, EC_{50} , 279.5 μM (183.0–426.8); n_H , 1.0 ± 0.1 , $n = 5$]. **C**, Schild plot analysis of the data from **B** yielded a regression slope of 0.74 ± 0.03 and a pA_2 value of 6.96 (negative x -axis intercept). Linear regression analysis shows no significant deviation from linearity ($r^2 = 0.996$). The dotted gray line indicates a regression slope of 1.

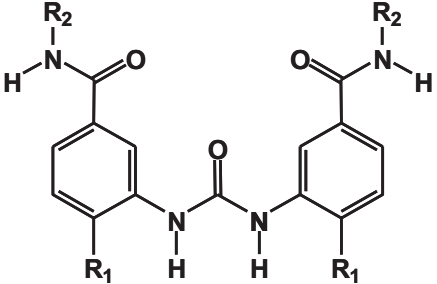
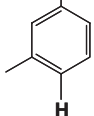
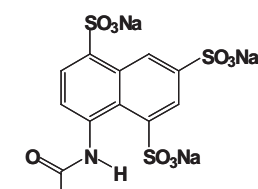
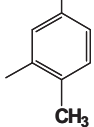
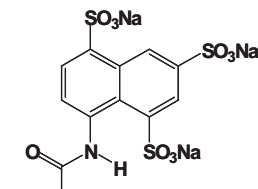
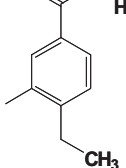
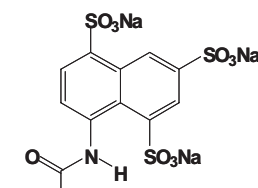
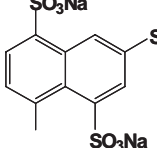
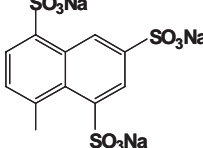
using the zfP2X4 receptor X-ray structure as a template. Because the zfP2X4 receptor structure has been solved in the absence of bound ATP, the exact location of the ATP-binding

pocket is unknown. However, by interpreting the zfP2X4 receptor structure in the context of functional mutagenesis data, it has been inferred that each of the three ATP-binding pockets

TABLE 2

Chemical structures of suramin derivatives and their IC₅₀ values at the rP2X2 receptor

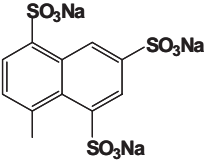
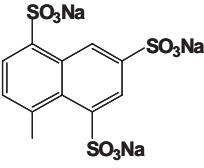
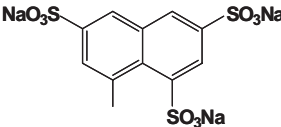
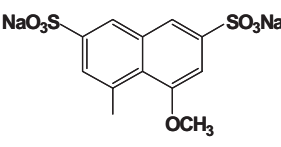
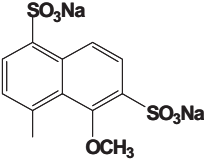
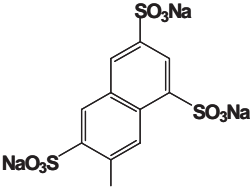
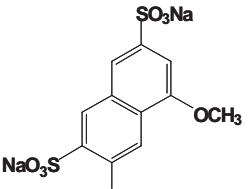
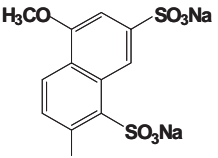
IC₅₀ values were derived from concentration–inhibition curves established with the steady-state protocol detailed in Fig. 1A. For suramin derivatives that have been described in previous articles or analyzed in detail in the present study, the corresponding chemical name is given in the footnote or in the text.

Compound (Derivative)		R ₁	R ₂	IC ₅₀ (95% CI) μM
				
1 (NF037)	H			0.28 (0.22–0.35)
2 (Suramin)	H			0.49 (0.47–0.52)
3 (NF127)	H			0.32 (0.29–0.36)
4 (NF023)	H			12.9 (5.9–27.7)

per homotrimer is represented by a deep groove on the outside of the protein that is assembled from two complementary half-shells provided by two adjacent subunits (Kawate et al., 2009). A corresponding groove is also present in our P2X2 homology model and includes several basic residues (Lys69, Lys71, Lys308) and the 288NFR290 motif (Fig. 3A), which have all been impli-

cated in ATP binding (Ennion et al., 2000; Roberts and Evans, 2004; Fischer et al., 2007; Guerlet et al., 2008; Roberts et al., 2008). We selected a set of four suramin derivatives (NF742, NF769, NF770, and NF778) that were representative of the structural hallmarks described above. Our docking experiments revealed that the hydrophilic cavity formed

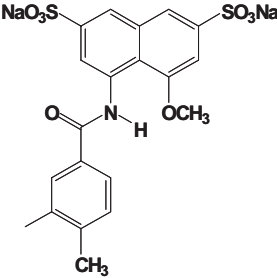
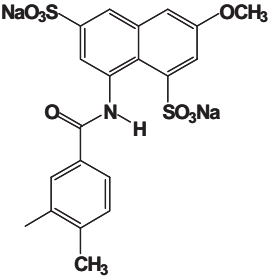
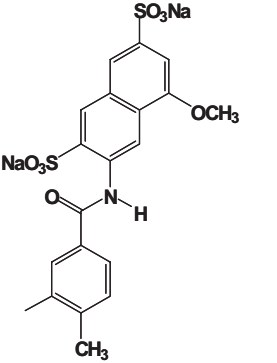
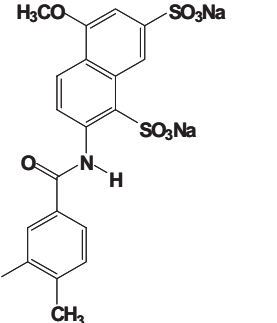
TABLE 2—Continued

Compound (Derivative)	R ₁	R ₂	IC ₅₀ (95% CI) <i>μM</i>
5 (NF058)	CH ₃		14.4 (7.7–26.9)
6 (NF124)	CH ₂ -CH ₃		9.9 (5.8–16.7)
7 (NF248)	CH ₃		22.8 (14.2–28.4)
8 (NF739)	CH ₃		5.1 (4.5–5.7)
9 (NF755)	CH ₃		10.9 (3.6–22.1)
10 (NF252)	CH ₃		4.6 (1.1–8.7)
11 (NF769)	CH ₃		1.3 (1.1–1.4)
12 (NF776)	CH ₃		0.097 (0.084–0.114)

between two adjacent subunits of the homotrimer, presumed to represent the ATP-binding site, was large enough to accommodate any of the four suramin derivatives, including the large urea derivative NF770 (Fig. 3A). The perfect fit enabled the NF770 molecule to interact

with residues both deep in the ATP-binding pocket and in the outer sphere (Fig. 3A). The interactions of NF770 are summarized in a two-dimensional (2D) ligand plot (Fig. 3C) that shows the Gaussian contact surfaces within a radius of 4.5 Å around the atoms of the ligands. Corre-

TABLE 2—Continued

Compound (Derivative)	R ₁	R ₂	IC ₅₀ (95% CI) μM
13 (NF742)	H		22.1 (14.1–27.1)
14 (NF763)	H		0.65 (0.39–1.11)
15 (NF770)	H		0.019 (0.016–0.022)
16 (NF778)	H		0.14 (0.121–0.161)

95% CI, 95% confidence interval.

Chemical names for compounds not already given in text: NF037, 8,8'-(Carbonylbis(imino-3,1-phenylenecarbonylimino-3,1-phenylenecarbonylimino))bis(naphthalene-1,3,5-trisulfonic acid) hexasodium salt; suramin, 8,8'-(carbonylbis(imino-3,1-phenylenecarbonylimino-3,1-(4-methylphenylene)carbonylimino))bis(naphthalene-1,3,5-trisulfonic acid) hexasodium salt; NF023, 8,8'-(carbonylbis(imino-3,1-phenylenecarbonylimino))bis(naphthalene-1,3,5-trisulfonic acid) hexasodium salt; NF058, 8,8'-(carbonylbis(imino-3,1-(4-methylphenylene)carbonylimino))bis(naphthalene-1,3,5-trisulfonic acid) hexasodium salt; NF124, 8,8'-(carbonylbis(imino-3,1-(4-ethylphenylene)carbonylimino))bis(naphthalene-1,3,5-trisulfonic acid) hexasodium salt; NF248, 8,8'-(carbonylbis(imino-3,1-(4-methylphenylene)carbonylimino))bis(naphthalene-1,3,6-trisulfonic acid) hexasodium salt; NF755, 8,8'-(carbonylbis(imino-3,1-(4-methylphenylene)carbonylimino))bis(1-methoxynaphthalene-2,5-disulfonic acid) tetrasodium salt; NF252, 7,7'-(carbonylbis(imino-3,1-(4-methylphenylene)carbonylimino))bis(naphthalene-1,3,6-trisulfonic acid) hexasodium salt; NF763, 8,8'-(carbonylbis(imino-3,1-phenylenecarbonylimino-3,1-(4-methylphenylene)carbonylimino))bis(3-methoxynaphthalene-1,6-disulfonic acid) tetrasodium salt.

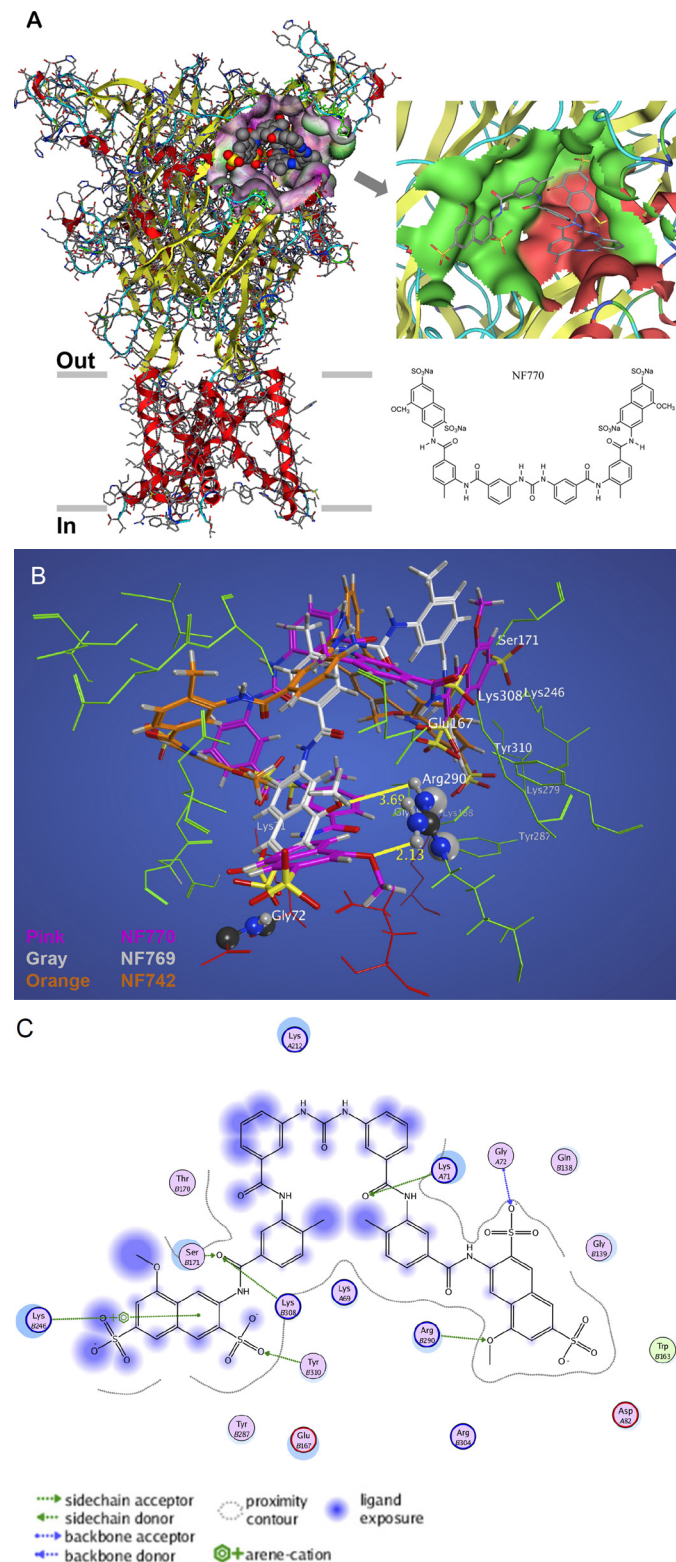


Fig. 3. Homology model of the rP2X₂ with NF770 and related compounds bound within the modeled ATP-binding pocket. **A**, stereoview of the homology-modeled homotrimeric rP2X₂ receptor structure with the docked NF770 as viewed from the side (i.e., parallel to the membrane plane). One of three ATP-binding sites located between neighboring subunits is highlighted with one NF770 molecule bound. β -Sheets are depicted in yellow, α -helical structures are in red, and random coil regions are in cyan. The gray bars mark the presumed boundaries of the outer (out) and inner (in) leaflets of the membrane bilayer. The ATP-binding pocket consists primarily of hydrophilic residues (indicated in pink), suggesting that polar substituents of the ligand are involved in strong

sponding 2D ligand plots of NF769, NF742, and NF778 are shown in Supplemental Fig. 1, A to C.

We then determined which amino acid residues are involved in ligand binding without explicitly determining the differing binding energies of the four compounds. We identified three residues, Lys279, Lys246 and Lys71, that formed hydrogen bonds with the acidic groups of the suramin derivatives (Fig. 3, B and C, and Supplemental Fig. 1, A–D) in a manner similar to that suggested for the interaction with the phosphate oxygens of ATP (Wilkinson et al., 2006; Roberts et al., 2008).

The most important differences in the binding modes, which determine the binding energy and the block of ATP function, resulted from the differences in the interactions with residues Gly72, Arg290, and/or Glu167. Although NF778 interacted with Gly72 and Glu167 (Supplemental Fig. 1, C and D), NF770 and NF769 interacted with Gly72 and Arg290 (Fig. 3B). In contrast, the 20- to 1000-fold less potent NF742 did not interact with any of these residues (Fig. 3B). Moreover, NF742 was incapable of forming a potency-determining interaction with residues other than Lys71, Lys246, and Lys279, which contribute equal binding energies for all the compounds. Therefore, NF742 cannot block ATP binding as potently as NF769, NF770, or NF778.

In our model, the oxygen of the methoxy group of NF770 is 2.1 Å from Arg290 (acceptor-hydrogen distance), thus enabling the formation of a strong, direct hydrogen bond, which contributes crucially to the free binding enthalpy and is essential for blocking the ATP from binding. In the less potent small urea NF769, the methoxy group and Arg290 are ~3.7 Å apart. This interaction may be mediated by a bridging water molecule,

binding. Neutral and hydrophobic residues are indicated in white and green, respectively. Inset, close-up view of the docking of NF770 into the ATP-binding pocket. One NF770 molecule (shown in stick representation) interacts with residues of two adjacent subunits (colored in green and red) that form the ATP-binding pocket. The binding pocket is large enough to accommodate the entire large urea derivative NF770, thus allowing NF770 to interact with residues deep within the ATP-binding pocket and in the outer sphere. Specific atoms of NF770 are colored by element type: carbons and hydrogens, dark gray; sulfur, yellow; oxygen, red; and nitrogen, dark blue. The planar structure of NF770 is shown at the bottom. **B**, comparison of the binding modes of NF770, NF769, and NF742. The suramin derivatives NF770 (pink), NF769 (gray), and NF742 (orange) in their lowest-energy conformations are superimposed within the rP2X₂ receptor binding pocket as obtained by docking to our homology model. Selected residues of the rP2X₂ receptor binding site are shown as green sticks, whereas the side chains of Gly72 and Arg290 are shown as balls and sticks. Specific atoms of the ligands are colored as detailed in **A**. NF770 and NF769, which both carry the naphthalene moiety in the 7,7' position relative to the amine group, are directed by a Gly72-sulfonate group interaction to orient spatially so that their methoxy group comes into close apposition to Arg290. As a result, a hydrogen bond can be formed that, according to our modeling data, is a key determinant of the interaction of NF769 and NF770 with the rP2X₂ receptor. The close distance of 2.13 Å between the methoxy group and Arg290 (yellow bar) seems to account for the stronger binding and higher potency of NF770 compared with NF769, the methoxy group of which is 3.69 Å from Arg290 (yellow bar). NF742 lacks this interaction and partially protrudes from the binding pocket because its 8,8'-positioned naphthalene moiety is conformationally less flexible than that of NF770 and NF769. As a result, NF742 is a much weaker blocker of the rP2X₂ receptor (IC_{50} , >20 μ M) than NF770 (IC_{50} , 19 nM). **C**, 2D interaction plot of NF770 within the rP2X₂ binding pocket. The molecular contacts between the ATP-binding pocket formed by two subunits (**A** and **B**) and NF770, as derived from our homology model and the identified binding mode of the ligand, are shown. Interacting residues are designated with letters **A** and **B** to indicate subunits **A** and **B**, respectively. Corresponding 2D plots of NF769 and NF742 within the binding pocket are shown in Supplemental Fig. 1, **A** and **B**.

which weakens the electrostatic effect with regard to the binding energy and steric hindrance for ATP binding.

Comparing NF770 and NF778, which differ only in the positions of the sulfonic acid and methoxy groups at the naphthalene moiety, shows different interaction modes in our homology model-based docking experiments (Supplemental Fig. 1, C and D). The strong hydrogen bond-based interaction of NF770 with Arg290 that crucially determines the binding energy is replaced in NF778 by a weaker interaction of the methoxy group with the backbone of Glu167 (Supplemental Fig. 1, C and D). This is due to the different substitution pattern of NF778 (1-methoxy-3,5-disulfonic acid) compared with NF770 (1-methoxy-3,6-disulfonic acid). In addition, the intraligand spatial orientation of the functional groups is important for the fixation of the ligand conformation. This is apparent, for instance, from a comparison of the 7,7' and 8,8' aminonaphthalene derivatives, which shows that the position of the naphthalene linkage affects the distance of the methoxy group to the amide moiety. A larger distance, such as the one in the 7,7'-aminonaphthalene derivatives NF769 and NF770, enhances the flexibility of the linkage and allows for a better fit within the ligand-binding pocket and tighter ligand binding.

Contribution of Gly72 and Glu167 to ATP Potency. Although the role of Arg290 in ATP binding to P2X2 receptors is already well documented (Guerlet et al., 2008; Roberts et al., 2008), a contribution of Gly72 and Glu167 has not been observed previously. To functionally verify the importance of these residues for ATP binding, we expressed single point mutants of the rP2X2 receptor in *X. laevis* oocytes and recorded the ATP-gated cation currents with TEVC. ATP concentration-response analysis of the G72A-rP2X2 receptor revealed a ~3-fold decrease in the maximal current amplitudes and a >13-fold increase in the EC₅₀ value from 18.5 (14.5–23.6) μ M (Fig. 4B, wild-type) to 244 (212–271) μ M (Fig. 4B, G72A mutant). The E167A-rP2X2 receptor exhibited virtually identical maximal current amplitudes but a ~5-fold decrease in the EC₅₀ value compared with the wt-rP2X2 receptor (Fig. 4B). The current shape (Fig. 4A), trimeric assembly (data not shown) and cell surface expression of both the G72A and the E167A mutant P2X2 receptor were unaffected compared with the wt-rP2X2 receptor (Fig. 4C). Mutant Arg290, corresponding to Arg298 in zP2X4, was analyzed as a positive control. Consistent with its crucial role in ATP binding (Guerlet et al., 2008; Roberts et al., 2008; Kawate et al., 2009), the R290A mutation resulted in an ~16-fold decrease in the maximal current amplitudes and a 27-fold increase in the EC₅₀ value compared with the wt-rP2X2 receptor (Fig. 4B). The current shape (Fig. 4A), trimeric assembly (data not shown), and cell surface expression (Fig. 4C) were unchanged. These data indicate that ATP binding is crucially determined by the same amino acid residues that were identified by homology modeling to determine the potency of suramin derivatives at the rP2X2 receptor.

Discussion

NF770 Is A Nanomolar-Potent P2X2 Receptor Antagonist. We used TEVC to show that the divalent suramin analog NF770 competitively inhibits recombinant P2X2 receptor subtypes expressed in *X. laevis* oocytes with an IC₅₀ value of 19 nM. To the best of our knowledge, NF770 repre-

sents the most potent rP2X2 receptor antagonist described so far. At the other P2X receptors, NF770 exhibits the following rank order of potencies based on IC₅₀ values: wt-rP2X2 \geq rP2X2-X3 \geq wt-rP2X2/3 > wt-rP2X3 > rP2X2-X1 > wt-rP2X1 > wt-rP2X4, wt-rP2X7.

NF770 is >50-fold more potent than the P2X antagonists that are currently regarded to be the most potent for the rP2X2 receptor: suramin, PPADS, and TNP-ATP. In addition, NF770 exhibits a ~10-fold selectivity for the P2X2 receptor over the P2X1 receptor. This suggests that NF770 has an advantageous profile compared with presently known compounds, which are nonselective with regard to P2X1 and P2X3 receptors (suramin and PPADS) or much more potent at the P2X1 and P2X3 receptor than at the P2X2 receptor (TNP-ATP) (Gever et al., 2006; Jarvis and Khakh, 2009). However, it remains unclear whether NF770 will inhibit the rP2X2 receptor in functional assays with the same high potency as on *X. laevis* oocytes. With the rP2X1 receptor-selective suramin derivatives NF449 and 8,8'-[carbonylbis(imino-4,1-phenylenecarbonylimino-4,1-phenylenecarbonylimino)]bis-1,3,5-naphthalenetrisulfonic acid hexasodium salt (NF279), for instance, we observed a markedly reduced potency in the isolated rat vas deferens compared with the oocyte-expressed rP2X1 receptor (Braun et al., 2001). In addition, the selectivity profile toward other receptors than P2X receptors has not yet been determined; therefore, effects mediated by other functionally important proteins in native tissues cannot be excluded.

The Inhibitory Potency of Suramin Derivatives Is Crucially Determined by Strong Polar Interactions within the ATP-Binding Pocket. Using structure-activity relationship analysis, we identified three structural determinants that contribute to efficient, competitive P2X2 receptor inhibition by suramin derivatives: 1) a "large urea" structure with two symmetric phenylenecarbonylimino groups linking the urea backbone with the naphthalene moiety, 2) using a β -aminonaphthalene moiety rather than a α -aminonaphthalene, and 3) the positioning of two sulfonic acid groups and a monomethoxy group at the naphthalene moiety. Our homology modeling-based ligand docking provides a uniform explanation of these findings. All of the changes to the chemical structures that increase the potency of the suramin derivatives at the rP2X2 receptor improve the spatial orientation within the ATP-binding pocket to allow for stronger polar interactions of functional groups (sulfonic acids or methoxy groups) with the amino acid residues important for ATP binding. First, the addition of a central phenylenecarbonylimino moiety reduces the acceptor-hydrogen distance between the oxygen of the methoxy group of NF770 and Arg290 from 3.7 to 2.1 Å, enabling the formation of a strong, direct hydrogen bond, which crucially determines the binding energy. Second, using a β -aminonaphthalene moiety rather than a α -aminonaphthalene places the methoxy group closer to the polar amino acid residues of the binding pocket (Arg290 and Glu167), resulting in an increase of the inhibitory potency at the rP2X2 receptor. Third, the different positions of the polar substituents at the naphthalene moiety affect the interaction modes within the ATP-binding site. In NF770, the interaction of one of the two sulfonic acid groups with Gly72 places the methoxy group in an orientation that enables it to form a strong hydrogen bond with Arg290. In NF778, only a weaker interaction with the backbone of Glu167 is feasible, thus explaining its ~7-fold potency compared with NF770.

Finally, also interligand interactions contribute to ligand potency. Certain positions of the naphthalene linkage and the substituents at the naphthalene moiety favor a closer proximity of the amide linker with the polar substituents. Consequently, the free rotatability of the naphthalene moiety at the amide linker is significantly reduced, resulting in a partial conformational fixation that hinders the optimal fitting of the ligand into the binding pocket.

Homology Docking Identifies Two Novel P2X2 Receptor Residues Involved in ATP Binding. Our homology docking assigned, for the first time, a role in ligand binding to the residues Gly72 and Glu167. This finding

rP2X2 and corresponding residues of other P2X isoforms have been unequivocally shown to participate in ATP binding (Ennion et al., 2000; Roberts and Evans, 2004; Fischer et al., 2007; Guerlet et al., 2008; Roberts et al., 2008). Second, the pore region and the channel gate have been assigned to pre-TM and TM2 residues (Cao et al., 2009; Keceli and Kubo, 2009; Jiang et al., 2010; Kracun et al., 2010). In addition to Arg290, Lys69, Lys71, and Lys308 (numbered according to the rP2X2 subunit), several phenylalanine and threonine residues are involved in the binding of ATP to P2X receptors, including P2X2 (Guerlet et al., 2008; Roberts et al., 2008), P2X1 (Ennion et al., 2000; Roberts and Evans, 2004), and

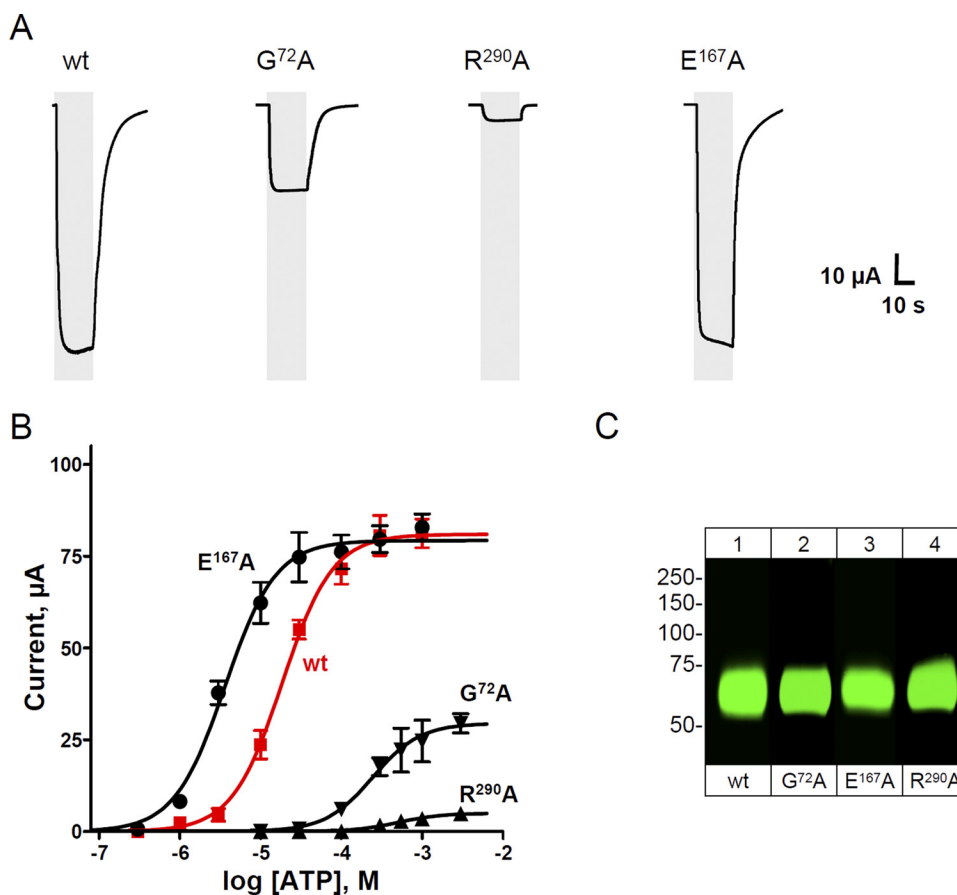


Fig. 4. Effect of mutation of Gly72, Glu167, or Arg290 of the rP2X2 receptors on ATP potency. A, representative original current traces elicited by 1 mM ATP (gray area) of the indicated wild-type or mutant rP2X2 receptors demonstrate that the nondesensitizing behavior is unchanged, whereas the maximal current amplitudes are altered. B, ATP concentration-response curves. Absolute current amplitudes are indicated. Red \blacksquare , wt-rP2X2, EC₅₀, 18.5 (95% confidence interval, 14.5–23.6) μ M; n_H , 1.4 ± 0.2 , $n = 12$; \blacktriangledown , G⁷²A-rP2X2, EC₅₀, 243.6 (212.1–271.3) μ M; n_H , 1.5 ± 0.4 , $n = 8$; \blacktriangle , R²⁹⁰A-rP2X2, EC₅₀, 504.8 (412.3–603.1) μ M; n_H , 1.6 ± 0.7 , $n = 8$; \bullet , E¹⁶⁷A-rP2X2, EC₅₀, 3.6 (2.7–4.9) μ M; n_H , 1.4 ± 0.2 , $n = 8$. C, [³⁵S]Methionine-labeled oocytes were chased for 24 h and surface-labeled with the membrane-impermeant fluorescent Cy5 dye before protein purification by nickel-nitrilotriacetic acid chromatography. Samples were resolved by reducing SDS-urea-PAGE and visualized in their Cy5-labeled surface form by fluorescence scanning. Numbers in left margin indicate the molecular masses of the marker proteins (in kilodaltons).

was verified functionally with single alanine substitutions of Gly72 and Glu167 that resulted in marked changes in ATP potency and, in the case of Gly72, in the maximum current amplitude. These data indirectly but strongly support the versatility of our homology model of the rP2X2 receptor, particularly for the presumed ATP-binding pocket.

We suggest that Gly72, Glu167, and Arg290 are directly involved in ligand binding rather than in channel gating. First, corresponding residues of the zfP2X4 receptor are all located within the suggested ATP-binding site, and Arg290 of

P2X3 (Fischer et al., 2007). To the best of our knowledge, our work is the first to demonstrate that Gly72 and Glu167 are potency-determining residues for competitive P2X2 receptor antagonism and are crucially involved in ATP binding. A similar role in ligand binding is also true for Arg290, which has already been identified in previous studies to be involved in ATP binding (Ennion et al., 2000; Roberts and Evans, 2004; Fischer et al., 2007; Guerlet et al., 2008; Roberts et al., 2008). The identification of Gly72-driven ligand orientation inside of the binding pocket is of significant interest for molecular ligand design or lead optimization.

Acknowledgments

We thank Ursula Braam for expert technical assistance in the molecular biology experiments.

Authorship Contributions

Participated in research design: Kless, Bahrenberg, Schmalzing, and Hausmann.

Conducted experiments: Wolf, Rosefort, Fallah, Bodnar, Wang, and Kless.

Contributed new reagents or analytic tools: Kassack and Hamacher.

Performed data analysis: Wolf, Illes, Kless, Bahrenberg, and Hausmann.

Wrote or contributed to the writing of the manuscript: Schmalzing and Hausmann.

Other: Schmalzing and Hausmann acquired funding for the research.

References

- Aschrafi A, Sadtler S, Niculescu C, Rettinger J, and Schmalzing G (2004) Trimeric architecture of homomeric P2X2 and heteromeric P2X1+2 receptor subtypes. *J Mol Biol* **342**:333–343.
- Becker D, Woltersdorf R, Boldt W, Schmitz S, Braam U, Schmalzing G, and Markwardt F (2008) The P2X7 carboxyl tail is a regulatory module of P2X7 receptor channel activity. *J Biol Chem* **283**:25725–25734.
- Braun K, Rettinger J, Ganso M, Kassack M, Hildebrandt C, Ullmann H, Nickel P, Schmalzing G, and Lambrecht G (2001) NF449: a subnanomolar potency antagonist at recombinant rat P2X1 receptors. *Naunyn Schmiedeberg's Arch Pharmacol* **364**:285–290.
- Brotherton-Pleiss CE, Dillon MP, Ford AP, Gever JR, Carter DS, Gleason SK, Lin CJ, Moore AG, Thompson AW, Villa M, et al. (2010) Discovery and optimization of RO-85, a novel drug-like, potent, and selective P2X3 receptor antagonist. *Bioorg Med Chem Lett* **20**:1031–1036.
- Burnstock G (2004) Introduction: P2 receptors. *Curr Top Med Chem* **4**:793–803.
- Burnstock G (2008) Purinergic signalling and disorders of the central nervous system. *Nat Rev Drug Discov* **7**:575–590.
- Cao L, Broomhead HE, Young MT, and North RA (2009) Polar residues in the second transmembrane domain of the rat P2X2 receptor that affect spontaneous gating, unitary conductance, and rectification. *J Neurosci* **29**:14257–14264.
- Cockayne DA, Dunn PM, Zhong Y, Rong W, Hamilton SG, Knight GE, Ruan HZ, Ma B, Yip P, Nunn P, et al. (2005) P2X2 knockout mice and P2X2/P2X3 double knockout mice reveal a role for the P2X2 receptor subunit in mediating multiple sensory effects of ATP. *J Physiol* **567**:621–639.
- Duckwitz W, Hausmann R, Aschrafi A, and Schmalzing G (2006) P2X5 subunit assembly requires scaffolding by the second transmembrane domain and a conserved aspartate. *J Biol Chem* **281**:39561–39572.
- Ennion S, Hagan S, and Evans RJ (2000) The role of positively charged amino acids in ATP recognition by human P2X₁ receptors. *J Biol Chem* **275**:29361–29367.
- Finger TE, Danilova V, Barrows J, Bartel DL, Vigers AJ, Stone L, Hellekant G, and Kinnamon SC (2005) ATP signaling is crucial for communication from taste buds to gustatory nerves. *Science* **310**:1495–1499.
- Fischer W, Zadori Z, Kullnick Y, Gröger-Arndt H, Franke H, Wirkner K, Illes P, and Mager PP (2007) Conserved lysin and arginin residues in the extracellular loop of P2X₃ receptors are involved in agonist binding. *Eur J Pharmacol* **576**:7–17.
- Gever JR, Cockayne DA, Dillon MP, Burnstock G, and Ford AP (2006) Pharmacology of P2X channels. *Pflugers Arch* **452**:513–537.
- Gever JR, Soto R, Henningsen RA, Martin RS, Hackos DH, Panicker S, Rubas W, Oglesby IB, Dillon MP, Milla ME, et al. (2010) AF-353, a novel, potent and orally bioavailable P2X3/P2X2/3 receptor antagonist. *Br J Pharmacol* **160**:1387–1398.
- Guerlet G, Taly A, Prado de Carvalho L, Martz A, Jiang R, Specht A, Le Novère N, and Grutter T (2008) Comparative models of P2X2 receptor support inter-subunit ATP-binding sites. *Biochem Biophys Res Commun* **375**:405–409.
- Hausmann R, Rettinger J, Gerevich Z, Meis S, Kassack MU, Illes P, Lambrecht G, and Schmalzing G (2006) The suramin analog 4,4',4''-(carbonylbis(imino-5,1,3-benzenetriylbis(carbonylimino)))tetra-kis-benzenesulfonic acid (NF110) potently blocks P2X3 receptors: subtype selectivity is determined by location of sulfonic acid groups. *Mol Pharmacol* **69**:2058–2067.
- Henikoff S and Henikoff JG (1992) Amino acid substitution matrices from protein blocks. *Proc Natl Acad Sci USA* **89**:10915–10919.
- Jahangir A, Alam M, Carter DS, Dillon MP, Bois DJ, Ford AP, Gever JR, Lin C, Wagner PJ, Zhai Y, et al. (2009) Identification and SAR of novel diaminopyrimidines. Part 2: the discovery of RO-51, a potent and selective, dual P2X(3)/P2X(2/3) antagonist for the treatment of pain. *Bioorg Med Chem Lett* **19**:1632–1635.
- Jarvis MF (2010) The neural-glial purinergic receptor ensemble in chronic pain states. *Trends Neurosci* **33**:48–57.
- Jarvis MF, Burgard EC, McGaraughty S, Honore P, Lynch K, Brennan TJ, Subieta A, Van Biesen T, Cartmell J, Bianchi B, et al. (2002) A-317491, a novel potent and selective non-nucleotide antagonist of P2X3 and P2X2/3 receptors, reduces chronic inflammatory and neuropathic pain in the rat. *Proc Natl Acad Sci USA* **99**:17179–17184.
- Jarvis MF and Khakh BS (2009) ATP-gated P2X cation-channels. *Neuropharmacology* **56**:208–215.
- Jiang R, Martz A, Gonin S, Taly A, de Carvalho LP, and Grutter T (2010) A putative extracellular salt bridge at the subunit interface contributes to the ion channel function of the ATP-gated P2X2 receptor. *J Biol Chem* **285**:15805–15815.
- Kassack MU, Braun K, Ganso M, Ullmann H, Nickel P, Böing B, Müller G, and Lambrecht G (2004) Structure-activity relationships of analogues of NF449 confirm NF449 as the most potent and selective known P2X1 receptor antagonist. *Eur J Med Chem* **39**:345–357.
- Kawate T, Michel JC, Birdsong WT, and Gouaux E (2009) Crystal structure of the ATP-gated P2X(4) ion channel in the closed state. *Nature* **460**:592–598.
- Keceli B and Kubo Y (2009) Functional and structural identification of amino acid residues of the P2X2 receptor channel critical for the voltage- and [ATP]-dependent gating. *J Physiol* **587**:5801–5818.
- Khakh BS, Gittermann D, Cockayne DA, and Jones A (2003) ATP modulation of excitatory synapses onto interneurons. *J Neurosci* **23**:7426–7437.
- Kracun S, Chaptal V, Abramson J, and Khakh BS (2010) Gated access to the pore of a P2X receptor: structural implications for closed-open transitions. *J Biol Chem* **285**:10110–10121.
- Labute P (2008) The generalized Born/volume integral implicit solvent model: estimation of the free energy of hydration using London dispersion instead of atomic surface area. *J Comput Chem* **29**:1693–1698.
- Labute P (2009) Protonate3D: assignment of ionization states and hydrogen coordinates to macromolecular structures. *Proteins* **75**:187–205.
- Needleman SB and Wunsch CD (1970) A general method applicable to the search for similarities in the amino acid sequence of two proteins. *J Mol Biol* **48**:443–453.
- Nicke A, Bäumer HG, Rettinger J, Eichele A, Lambrecht G, Mutschler E, and Schmalzing G (1998) P2X1 and P2X3 receptors form stable trimers: a novel structural motif of ligand-gated ion channels. *EMBO J* **17**:3016–3028.
- Rettinger J, Braun K, Hochmann H, Kassack MU, Ullmann H, Nickel P, Schmalzing G, and Lambrecht G (2005) Profiling at recombinant homomeric and heteromeric rat P2X receptors identifies the suramin analogue NF449 as a highly potent P2X1 receptor antagonist. *Neuropharmacology* **48**:461–468.
- Roberts JA, Digby HR, Kara M, El Ajouz S, Sutcliffe MJ, and Evans RJ (2008) Cysteine substitution mutagenesis and the effects of methanethiosulfonate reagents at P2X2 and P2X4 receptors support a core common mode of ATP action at P2X receptors. *J Biol Chem* **283**:20126–20136.
- Roberts JA and Evans RJ (2004) ATP binding at human P2X1 receptors. Contribution of aromatic and basic amino acids revealed using mutagenesis and partial agonists. *J Biol Chem* **279**:9043–9055.
- Rong W, Gourine AV, Cockayne DA, Xiang Z, Ford AP, Spyer KM, and Burnstock G (2003) Pivotal role of nucleotide P2X2 receptor subunit of the ATP-gated ion channel mediating ventilatory responses to hypoxia. *J Neurosci* **23**:11315–11321.
- Summa CM and Levitt M (2007) Near-native structure refinement using in vacuo energy minimization. *Proc Natl Acad Sci USA* **104**:3177–3182.
- Surprenant A and North RA (2009) Signaling at purinergic P2X receptors. *Annu Rev Physiol* **71**:333–359.
- Trujillo CA, Nery AA, Martins AH, Majumder P, Gonzalez FA, and Ulrich H (2006) Inhibition mechanism of the recombinant rat P2X(2) receptor in glial cells by suramin and TNP-ATP. *Biochemistry* **45**:224–233.
- Ullmann H, Meis S, Hongwiset D, Marzian C, Wiese M, Nickel P, Communi D, Boeynaems JM, Wolf C, Hausmann R, et al. (2005) Synthesis and structure-activity relationships of suramin-derived P2Y11 receptor antagonists with nanomolar potency. *J Med Chem* **48**:7040–7048.
- Wilkinson WJ, Jiang LH, Surprenant A, and North RA (2006) Role of ectodomain lysines in the subunits of the heteromeric P2X2/3 receptor. *Mol Pharmacol* **70**:1159–1163.

Address correspondence to: Ralf Hausmann, Department of Molecular Pharmacology, University Hospital of RWTH Aachen University, Wendlingweg 2, D-52074 Aachen, Germany. E-mail: rhausmann@ukaachen.de